OPTOELECTRONICS AND ADVANCED MATERIALS – RAPID COMMUNICATIONS Vol. 7, No. 5-6, May – June 2013, p. 381 - 392

Structural and optical characterizations of nanocrystalline PbTe films prepared by flash evaporation and its device application

A. A. M. FARAG, F. S. TERRA[a], G. M. M. FAHIM[a], A. ASHERY[a], MAHMOUD NASR[a], M. M. EL OKR[b]
Thin Film laboratory, Physics Department, Faculty of Education, Ain Shams University
[a]Solid State Electronics lab, Physics Departement, Physics Division, National Research Center, Dokki, Giza, Egypt,
[b]Physics Department, Faculty of Science, Al-Azhar University, Nasr City. Cairo, Egypt

The flash evaporation technique was successfully used to deposit highly uniform, good adhesive and nearly stoichiometry PbTe thin films at substrate temperatures of 473 (sample 1) and 503 K (sample 2). The chemical composition of PbTe using energy dispersive X-ray (EDX) showed a nearly stoichiometric composition of sample 2 compared to that of sample 1.The transmission electron microscopy (TEM) results were in good agreement with the results of X-ray diffraction (XRD) analysis. Based on the use of the maxima and minima of the interference fringes, a straightforward analysis proposed by Swanepoel has been applied to derive the optical constants. The refractive index of PbTe thin films of sample 1 was low compared to that of sample 2. The optical transition responsible for optical absorption in the films was found to be direct allowed. The *C-V* characteristics of n-PbTe/p-Si at substrate temperatures of 473 (device 1) and 503 K (device 2) were studied at high frequency (1 MHz). The results showed that the main parameters such as the carrier concentration (N_A), the built-in potential (V_b), the barrier height (Φ_b), the width of space charge region (W) and the maximum electrical field (E_{max}) of device 1 are low compared to device 2. Moreover, the increase in the carrier concentration of the two devices with temperature in the range 300-375 K can be attributed to the decrease in the width of the depletion region.

(Received October 13, 2012; accepted June 12, 2013)

Keywords: Flash evaporation, Thin film, Opticalcharacteristics, Nanocrystalline PbTe, n-PbTe/p-Si device

1. Introduction

Binary IV–VI semiconducting compounds form a very interesting class of materials because of their potential applications in thermoelectric, electronic and optoelectronic devices due to their unique thermal and electrical properties [1-3]. Among the IV–VI class of materials, lead telluride (PbTe) and selenide (PbSe) have attracted great attention for their applications in thermoelectric power generations. PbTe is a kind of lead chalcogenide. It has a high melting point, good chemical stability, low vapor pressure and good chemical strength [4]. It also has found extensive usefulness in infrared (IR) optoelectronics for manufacturing IR lasers and detectors [5]. Moreover, it has an indirect band gap of ~ 0.29 eV [6], direct band gap of ~ 0.32 eV [7] and exhibited both p- or n-type conductivity [8]. Because of narrow band gap, PbTe is useful for optoelectronic devices in infrared wavelength region [9] and photoconductors [10]. Compared to other narrow band gap III–V or II–VI semiconductors PbTe has some unique properties like positive temperature coefficient, negative pressure coefficient, large refractive index and smaller Auger recombination rate [7, 11]. Due to its high carrier mobility and low thermal conductivity than that of other semiconductors it has much potential in thermo- electric applications [12, 13].

Various vacuum deposition techniques have been utilized to deposit PbTe thin films including molecular beam epitaxy (MBE) [14], magnetron sputtering (MS) [15], thermal evaporation (TE) [16-18], pulsed laser deposition (PLD) [19], electrodeposition (ED) [20] and flash evaporation (FE) [21-23]. The flash evaporation is suitable for the preparation of III/V films which preserved the stoichiometry in thin films [23]. However, to the best of our knowledge there has been very little research on the growth of n-PbTe/p-Sihetero structure by flash evaporation. Here we report the growth of PbTe thin films employing flash evaporation technique wherein we have overcome many of the problems associated with the growth by optimizing several parameters, such as III/V mass ratio and growth temperature. Moreover, an attempt to achieve a better understanding of the optical characteristics of PbTe thin films deposited at different substrate temperatures of 473 and 503 K was considered. Thedark current–voltage (*I-V*) and capacitance–voltage (*C-V*) characteristics at different temperatures for the n-PbTe/p-Si heterojunctions to obtain the important parameters and the predominant conduction mechanisms were also carried out.

2. Experimental

2.1.Thin film preparation

Although some limitation of the flash evaporation technique, it has attractive features [21-23]. By careful management, the difficulties can be overcome, and deposited films of splatter-free surface can be achieved. PbTe thin films were prepared onto glass, freshly cleaved NaCl crystal and single crystalline Si substrates held at a temperature of 473 and 503 K using a high vacuum coating unit (Edwards E 306 A, England). A rapid flash evaporation of a compound can be obtained by continuously dropping fine particles of the material onto a hot boat surface so that numerous discrete evaporation occurs. A sketch of the home-made flash evaporation attachment is depicted in Fig. 1. The evaporation (boat) temperature was kept constant at about 924 ^{o}C and the deposition rate has been controlled at a mean value of 2 nm s $^{-1}$ by the vibrator of the home-made flash evaporation attachment.

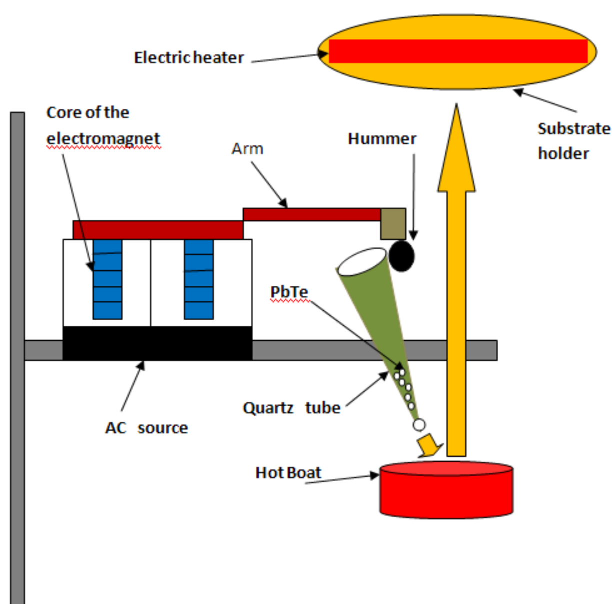

Fig. 1. A sketch of the home-made flash evaporation attachment.

Film thickness was measured by quartz-crystal for monitoring and controlling of the deposition rate as well as the thickness during film preparation by film thickness monitor (FTM4, Edward, England).

2.2. Characterization techniques

The structural properties of the films were investigated by X-ray diffraction (XRD). This technique was performed to study the crystal structure of the films using analytical X'Pertdiffractometer with CuK$_{\alpha}$ radiation. The film morphology was investigated by scanning electron microscopy (SEM) using JEOL type 8400 attached with energy dispersive X-ray,EDX unit with accelerating voltage 30 kV, magnification 10× up to 400,000× and 3.5 nm resolution for EDX.

Nanocrystalline of PbTe samples were examined and imaged using a JEOL JEM-1230 transmission electron microscope equipped with a GATAN multiscan camera operating at 120 kV. Samples for TEM were prepared by casting a drop of PbTe suspensions in anhydrous hexane onto a copper grid coated with Formvar/carbon at room temperature. The grid was horizontally placed on a piece of filter paper so that the solvent was absorbed by the paper as soon as the suspension was dropped, leaving the PbTe deposited on the grid.

The optical transmission of the PbTe films, deposited onto freshly cleaved NaCl substrates, were recorded in the spectral range from 2.5 to 11 μm,using a spectrophotometer model JASCO FT/IR-6100 type A,USA.

To form Au/PbTe/p-Si/Al heterojunction, gold electrode was first evaporated on PbTefilm through suitable mask to form a front ohmic electrode and aluminum was evaporated on p-Si as a back electrode. In order to measure the electrical properties of the heterojunction, electrical contacts were equipped with copper wires mechanically applied to the two metal electrodes using thermosetting silver paint. The dark current–voltage (*I–V*) measurements were performed at different temperatures by a high impedance programmable Keithley 617 source meter. The dark capacitance–voltage measurements were performed at different temperatures by maintaining a constant fixed frequency at 1 MHz, using a computerized capacitance–voltage system consisting of the 410 C–V meter via model 4108 C–V interface. The temperature was measured directly by means of *K*-type thermocouple connected to hand-held digital thermometer.

2.3. Crystallite size and internal strain calculation

It is well known that X-ray diffraction line broadening is influenced by the crystallite size and the internal strains. In order to obtain these parameters, Williamson-Hall method was used.

In nanomaterials both crystallite size and lattice strain have their own contribution to X-ray diffraction peak broadening and the peak broadening contributed by lattice strain is due to large volume of grain boundaries [24, 25]. In order to measure the correct crystallite size and to study the modifications introduced by strain in the properties of nanomaterial, strain calculations are required [25]. However, completely and accurately fitting for the powder diffraction data are complicated and hence it attracts many indirect methods such as Williamson– Hall method and Warren–Averbach analysis for estimating the lattice strain and crystallite size [24,25]. Williamson– Hall(W-H) analysis is a simplified method that clearly differentiates between size induced and strain induced peak broadening by considering the peak width as a function of 2θ.

The W-H method does not follow a $1/\cos\theta$ dependence as in the Scherrer equation but instead varies with $\tan\theta$. This fundamental difference allows for a separation of reflection broadening when both

microstructure causessmall crystallite size and microstrain, ε, occur together. The size and strain broadening are additive components of the total integral breadth of a Bragg peak [24]. The distinct θ dependencies of both effects laid the basis for the separation of size and strain broadening in theanalysis of W- H method.

In the W-H method, the analysis includes two steps: First step: the width$\beta_{exp}$of every peak was measured as the integral breadth. The instrumental broadening (β_{inst}) was determined from standard polycrystalline silicon. The peak breadth due to sample (strain + size), $\beta$was calculated according to Gaussian profile [24,25]:

$$\beta = \left(\beta_{\exp}^2 - \beta_{inst}^2\right)^{1/2} \tag{1}$$

Second step: the crystallite size and internal strain were obtained by fitting the Williamson-Hall equation [24, 25]:

$$\beta \cos\theta = \frac{K\lambda}{D} + 2\varepsilon \sin\theta \tag{2}$$

where D is the coherent scattering length (crystalline size), K is a constant whose value is approximately 0.9, $\beta$is the integral width of the sample (in rad.) calculated in the first step and $\varepsilon$is the inhomogeneous internal strain (in %).

2.3.Method of calculating optical constants

The optical system under consideration corresponds to homogeneous and uniform thin films, deposited on thick transparent substrates. The evaporated films have thickness (d) and complex refractive index ($n_c = n - ik$) , where n and k are the refractive and extinction indices, respectively. The thickness of the substrate is several orders of magnitude larger than d and its $n$is symbolized by s. The substrate is considered to be perfectly smooth, but thick enough so that in practice the planes are not perfectly parallel so that all interference effects arising from the substrate are destroyed. The system is surrounded by air with refractive index ($n_o = 1$). Taking all the multiple reflections at the three interfaces into account, it can be shown that in the case $k^2 << n^2$, the transmission T at normal incidence is given by [26]:

$$T = \frac{A\chi}{B - C\chi\cos\phi + D\chi^2} \tag{3}$$

where$A = 16n^2 s$, $B = (n + 1)^3\ (n + s^2)$, $C = 2(n^2 - 1)(n^2 - s^2)$, $D = (n - 1)^3(n - s^2)$, $\phi = 4\pi nd/\lambda$ and $\chi = \exp\ (-\alpha d)$. The values of the transmission at the maxima and minima of the interference fringes can be obtained from Eq. (3) by setting the interference condition cos $\phi = +1$ for maxima (T_M) and cos $\phi = -1$ for minima (T_m). The measured transmittance (T) spectra, the created envelopes T_M and T_m, in the spectral region with interference fringes of thin films were analyzed according to Swanepoel's method based on the idea of Manifacier et al. [27]. The first approximate value of the refractive index of the film, n_1, in the spectral region of medium and weak absorption can be calculated from the following expression:

$$n_1 = \sqrt{N + \left(N^2 - s^2\right)^{1/2}} \tag{4}$$

where

$$N = 2s\frac{T_M - T_m}{T_M T_m} + \frac{s^2 + 1}{2}, \tag{5}$$

hereT_M and T_m are respectively, the transmission maximum and the corresponding minimum at a certain wavelength. Alternatively, one of these values is an experimental interference maximum (or minimum) and the other one is derived from the corresponding envelope. Both envelopes being computer-generated using the OriginLab (version 7) program.

Since the values of the film thickness (d) and the refractive index (n) are already known over the whole spectral range 2.5-11 μm, then the extinction index can be obtained through the well known relationship:

$$k = \frac{\alpha\lambda}{4\pi} \tag{6}$$

The experimental error in measuring the film thickness was taken as ±2%, in T and R as ±1% and in the calculated values of n and k as 3% and 2.5%, respectively.

3. Results and discussion

3.1. Morphology and structural characteristics

It is important to investigate the surface morphology of the flash evaporated PbTe films, since the surface morphology of the PbTe thin films will further affect the optical and electrical characteristics. Figs. 2(a) and 3(a)show the scanning electron micrograph of the surface topography of the evaporated PbTe film grown on NaCl substrate prepared at temperature of 473 K (sample 1)and 503 K (sample 2), respectively. The surface image revealed that the PbTe thin films have a fine-grained nanostructure without cracks. Thin films of sample 2 has extremely small grain size and a smooth surface as compared with that for sample 1. It is reported that a small lattice mismatch of the thin film with the substrate leads to less grain boundary grooving, resulting in smooth surface morphology [28].

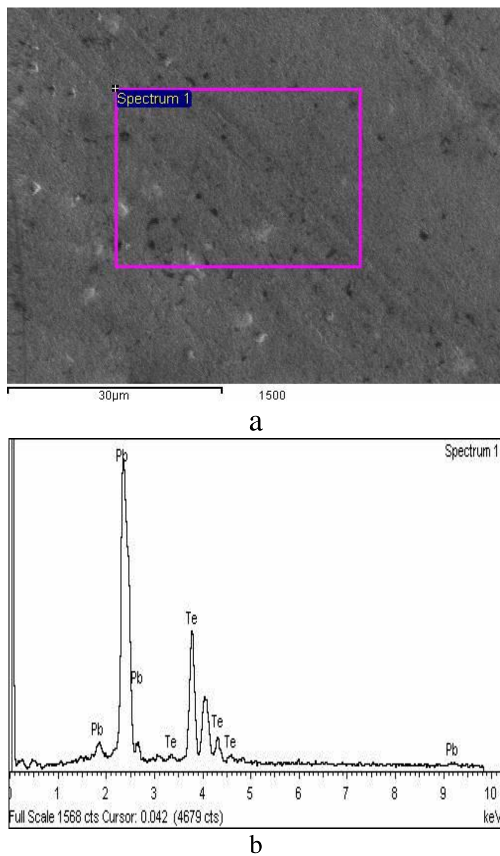

Fig. 2. a)SEM of PbTe film prepared at substrate temperature 473 K, b) EDX analysis.

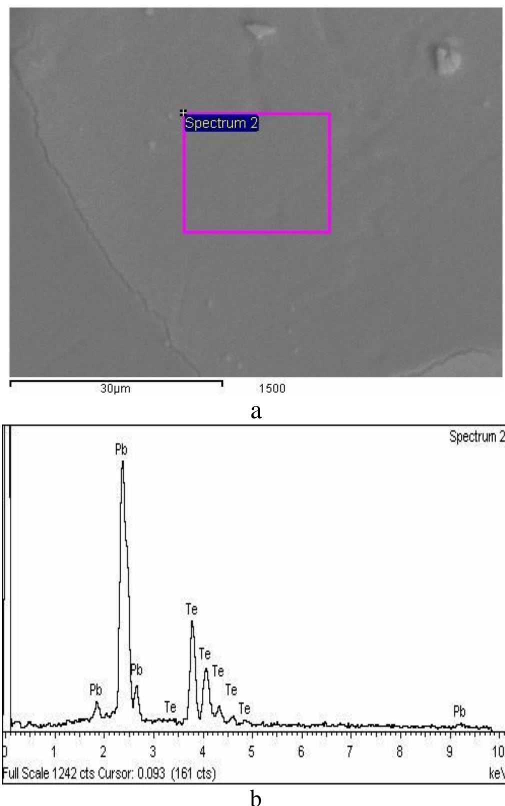

Fig. 3. a) SEM of PbTe film prepared at substrate temperature 503 K, b) EDX analysis.

The EDX analysis, shown in Figs. 2(b) and 3(b),for the PbTe films were measured at several surface positions of the investigated samples to determine their composition. The results of the EDX measurementsfor sample 1 and 2 are listed in Table 1 which represents the constituent elements percentage. As observed from the table that sample 2 is highly stoichiometric and very close to the ideal one of 1:1 as compared with that of sample 1.

Table 1. The results of weight percent of elements in PbTe by EDX.

	Weight %	
	Pb %	Te%
Sample 1	47.4 ±1.42	52.6 ±1.57
Sample 2	49.56 ±1.48	50.44 ±1.51

A typical transmission electron microscopy (TEM) image of nanocrystalline PbTe of sample 1 and 2 is shown in Fig. 4 (A) and (B). The observed nanocrystals do not display any definite shape and possess mostly spheroidal nanoparticle morphologies. Average nanoparticle diameters from TEM micrographs were determined to be 30-50 nm for both the two nanocrystalline PbTe samples.

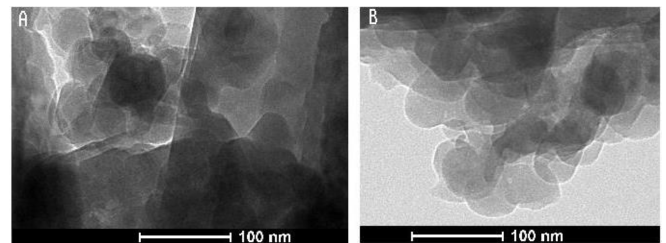

Fig. 4. TEM of PbTefilm prepared at different substrate temperature (A)473 K and (B)503 K.

X-ray diffraction pattern of sample 1 and 2 is shown in Figs. 5 (a) and (b). The XRD patterns exhibitthe reflections corresponding to the same face centered cubic system. Thus, the PbTe films deposited onto the NaCl substrates at temperature of 503 K is found to have more preferredorientation along (200) direction.The results are matched with the standard card JCPDS no.8-28 for PbTeas listed in Table 2. It is clearly observed a monocrystalline characteristic PbTe of sample 2 compared to that for sample 1 whichgives evidence for the effect of substrate temperature on the structural characteristics of flash evaporated PbTe films.

Table 2. Calculated and standards d- values ofPbTe and the corresponding hkl.

Calculated d-value	d-value using card no. (8-28)	(*hkl*)
3.225	3.231	(200)
2.281	2.282	(220)
1.863	1.858	(222)
1.614	1.609	(400)
1.318	1.314	(422)

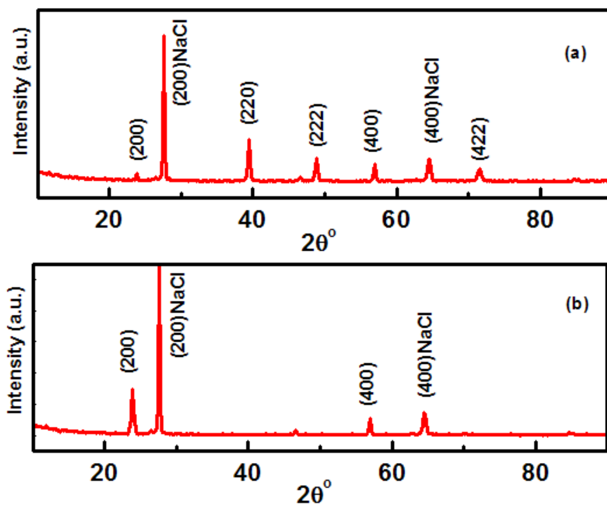

Fig. 5. XRD of PbTe film sevaporated on single crystalline NaCl substrate a) at substrate temperature 473 K, b) at substrate temperature 503 K.

The crystallite size and internal strain were estimated from the W-H method. The fivemost intensive reflection peaks of the sample1 and the two reflection peaks in the case of sample 2 were used in the line broadening analysis. Fig. 6 shows W-H plot for the sample 1. From this curve one can estimate the crystallitesize and the internal strain using the intercept and the slope of the fitted line, respectively. The obtained crystallite size and the internal strain for sample 1are large than those of sample 2 as listed in Table 3. As observed the average crystallite size of PbTe for samples 1 and 2 that deduced by W-H analysis are significantly larger than the number-averaged particle sizes determined by TEM.

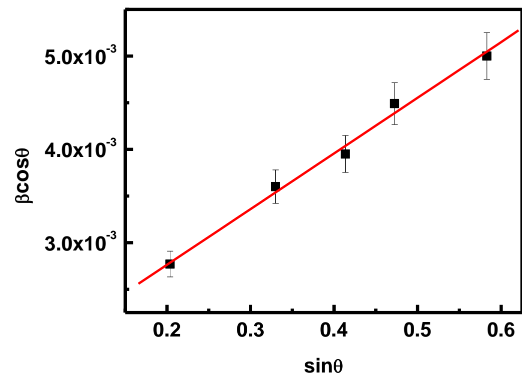

Fig. 6. $\beta \cos \theta$ vs. $\sin\theta$ of PbTe films evaporated on single crystalline NaCl substrate at substrate temperature 473 K.

Table 3. The mean crystallite size and the internal strain of PbTe film deduced by using Williamson– Hall (W-H) analysis.

	Crystallite size(D)	Internal strain(ε)
Sample 1	87 ±4.35 nm	0.295±0.014%
Sample 2	62 ±3.10 nm	0.094±0.004 %

3.2. Optical characteristics

Theoptical properties of samples 1 and 2 werestudied in the spectral range 400 to 4000 cm^{-1}. A spectrophotometer model FT/IR-6100typeA was applied for the transmittance measurements. Results presented here show the relative transmittance, i.e. the transmittance of a PbTe film deposited onto NaCl plate related to the transmittance of the same NaCl plate without any coating. Fig. 7 shows the dependence of the transmission (T) upon the wave number of samples 1 and 2. It is observed that the two films havelow transparency and characterized by interference.

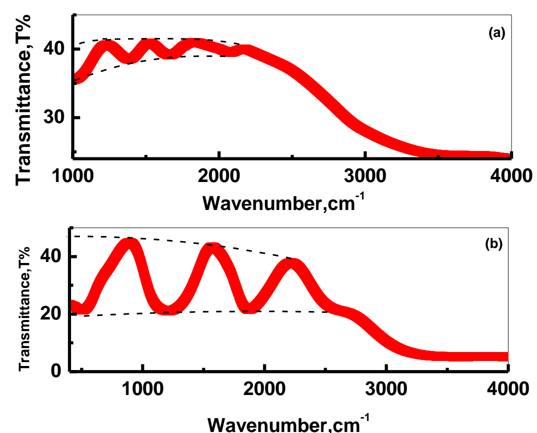

Fig. 7. Spectral dependence of transmittance of PbTe thin films a) at substrate temperature 473 K b) at substrate temperature 503 K.

3.3. Determination of theoptical constants of PbTe films

The refractive and extinction indices(n and k) were computed from the measured transmittance after correcting the substrate effect. Taking into account that the optical system under consideration corresponds to homogeneous and uniform thin films deposited on thick transparent substrates since the thickness of the substrates is several orders of magnitude larger than film thickness. Taking all the multiple reflections at the three interfaces into account, it can be shown that in the case $k^2 << n^2$, the transmission at normal incidence is given by Aly et al. [29].

The refractive index (n) can be calculated using the created envelopes, the maxima (T_M) and minima (T_m) in the measured transmittance spectrum. The measured refractive and extinction indices for samples 1 and 2 are shown in Figs. 8 and 9, respectively, according to Swanepoel's method based on the idea of Manifacier et al.[27]. It is observed that there is a dependence of both extinction and refractive indices on the photon energy for the two samples.

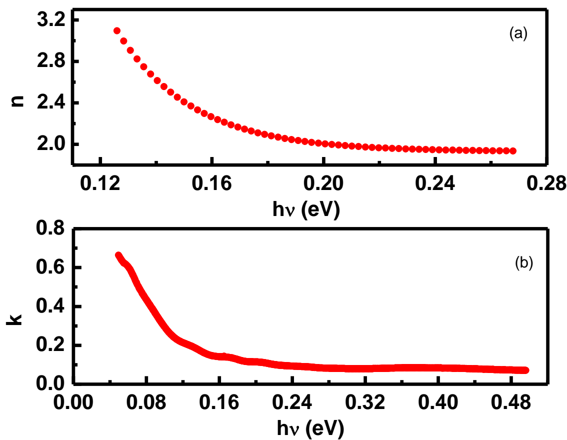

Fig. 8. Photon energy dependence of a) refractive index b) extinction index ofPbTe thin films at substrate temperature 473 K.

It is seen from Figs. 8 and 9 that the values of the refractive index obtained for sample 2 is matched with thatof reportedby Li et al. [30]. But the refractive index of sample 1 is lower than that of the published data. This may be attributed to the surface roughness of the deposited PbTe film which is disadvantageous to subsequent fabrication that affects the optical characteristics due to the presence of light scattering [31,32]. Other reason which can be considered may be attributed to the lower stoichiometry [31] of sample 1as comparedwith that of sample 2.

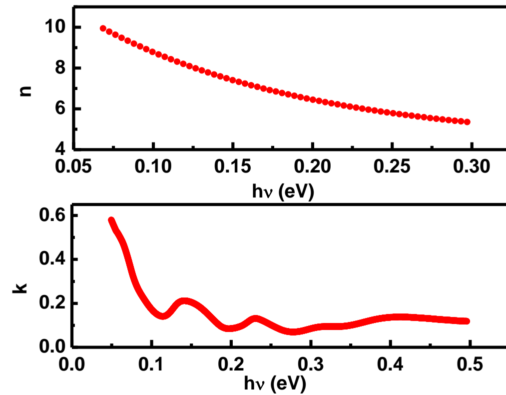

Fig. 9. Photon energy dependence of a)refractive index b) extinction index of PbTe thin films at substrate temperature 503 K.

3.4. Dielectric characterizations

For further analysis of the optical data a number of useful and associated relations can be derived to link the real and imaginary parts of the dielectric function and the optical constants (n, k). It is well known that the polarizabiltiy of any solid is proportional to its dielectric constant. The real and imaginary parts of the complex dielectric constant are expressed as [32]:

$$\varepsilon_1 = n^2 - k^2, \quad \text{and} \quad \varepsilon_2 = 2nk, \qquad (7)$$

where ε_1 and ε_2 are the real and imaginary parts of the dielectric constant, respectively. The dependences of ε_1 and ε_2 on the photon energy are shown in Figs. 10 and 11 for samples 1 and 2, respectively. The real and imaginary parts follow the same pattern but the values of the real part are higher than imaginary part. The variation of the dielectric constant with photon energy indicates some interactions between photons and electrons in the PbTe films. It is noticed that the real dielectric constant of sample 2 is high compared to that for sample 1 which may be attributed to the same factors affecting the refractive index as discussed above.

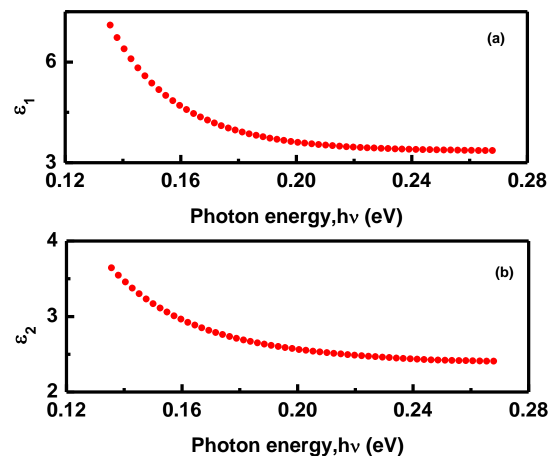

Fig. 10. Photon energy dependence of a) real dielectric constant b) imaginary dielectric constant of PbTe thin films at substrate temperature 473 K.

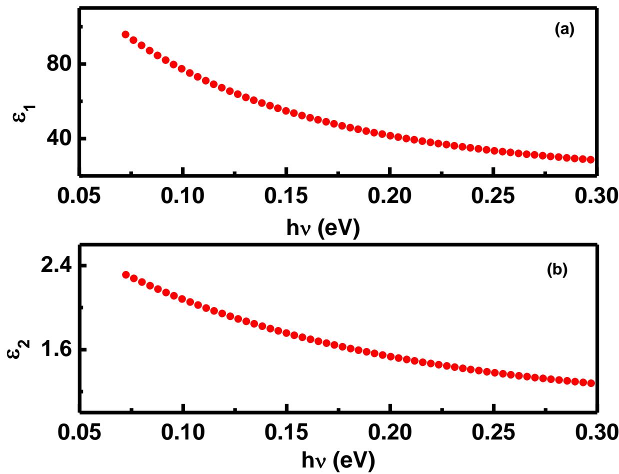

Fig. 11. Photon energy dependence of a) real dielectric constant, b) imaginary dielectric constant of PbTe thin films at substrate temperature 503 K.

3.5.Optical energy band gap characterization

The dependence of the absorption coefficient, α, on the photon energy, $h\nu$, is important to obtain information about the energy band structure and the type of optical transition. Mott and Davis [33] suggested the relation between the absorption coefficient and the incident photon energy as follows:

$$(\alpha h\nu)^r = B^\backslash (h\nu - E_g), \qquad (8)$$

where$B^\backslash$is constant, E_g is the optical energy gap and r is constant which characterizes the transition process. The constant r takes the values 2 for direct allowed transition, 2/3 for direct forbidden transitions, 1/2 for indirect allowed transition and 1/3 for indirect forbidden transitions. The usual method for the determination of the value of E_g involves plotting a graph of $(\alpha h\nu)^r$vs. $h\nu$. The dependence of $(\alpha h\nu)^r$ on photon energy $h\nu$ near the absorption edge was plotted for different values of r and it was found that the best fit was obtained at $r = 2$ as shown in Figs. 12(a) and (b) for samples 1 and 2, respectively. This behavior indicates that the transitions are direct allowed in the two samples that characterize PbTe films. The determined value of the direct band gap of sample 2 is matched with the published in the literature [34-36] and was found to be larger than that of obtained for sample 1. The decrease in the energy gap for sample 1as compared to that of sample 2 may be attributed to the same reasons discussed before [37].

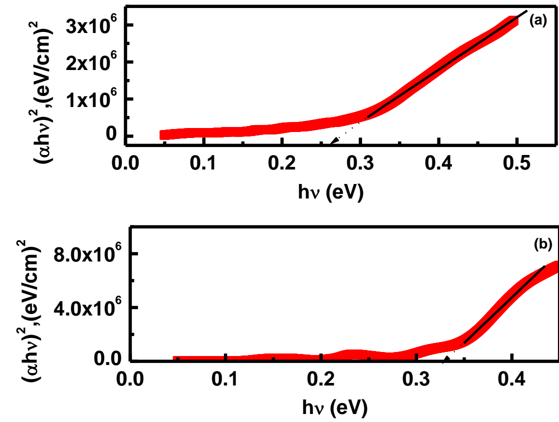

Fig. 12. Plot of $(\alpha h\nu)^2$ vs. $h\nu$ of PbTe thin films a) at substrate temperature 473 K b) at substrate temperature 503 K.

3.6. Capacitance –voltage characterization

The high frequency C–V characteristics of the typical devices n-PbTe/p-Si prepared by flash evaporation technique at substrate temperatures of 473 K (device1) and 503 K (device 2) are illustrated in Figs.13(a) and (b), respectively. The junction capacitance properties of the devices 1 and 2 are found to follow the similar variation; the capacitance decreases with increasing reverse bias but increases with increasing temperature in the range 300-375 K. This can be explained by the presence of n-PbTe/p-Si interface. The strong dependence of capacitance-voltage characteristics on temperature observed for all devices indicate the presence of interface states located at or near the junction interface [38].

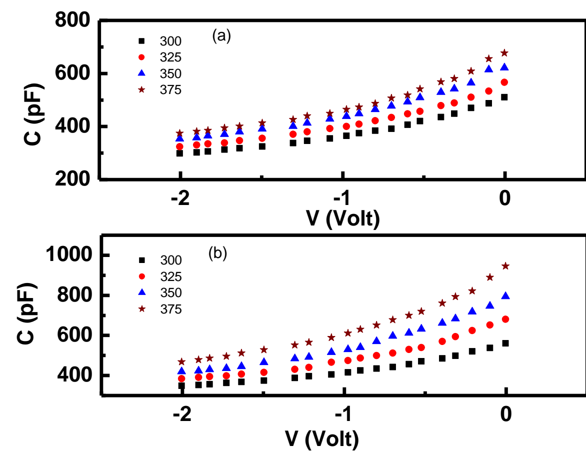

Fig. 13. Capacitance-voltage characteristics of PbTe/n-Si heterojunction in the temperature range 300-375 K a) at substrate temperature 473 K, b) at substrate temperature 503 K.

The depletion layer of a p-n junction can be discussed as a parallel plate capacitor, the depletion width (W)would

vary with bias voltage. The capacitance can be expressed as [38]

$$C=\left(\frac{\varepsilon\varepsilon_o A}{W}\right)=\left(\frac{\varepsilon\varepsilon_o A}{\left(\left(\frac{2\varepsilon\varepsilon_o}{q}\right)(V_b+V)(N_A+N_D)/(N_A N_D)\right)^{1/2}}\right), \quad (9)$$

Where N_A and N_D are the doping densities on the p and n sides respectively, V_b is the built-in potential and A is the effective area.

For a parabolic energy barrier of a Schottky diode [either (N_A>>N_D or (N_D >> N_A), the C-V relation can be written as

$$C=\left(\frac{2(V_b+V)}{\varepsilon\varepsilon_o qNA^2}\right)^{1/2} \quad (10)$$

Here $N=N_D$ when N_A>>$N_D$or $N=N_A$ when N_D >> N_A . The latter condition is valid for n-PbTe/p-Si junction diode. Eq. (9) indicates that the plot of $1/C^2$ vs. V would be a straight line and the slope would give the density of acceptors inside the space charge region usingε=11.8 for p-Si.The built-in potential (V_b) could be obtained from the intercept on the voltage axis. Figs. 14(a) and (b) show the above plots for the devices 1 and 2 respectively.

The approximate depletion width (W) may be obtained from the relation

$$W=\frac{\varepsilon\varepsilon_o}{C/A}=\left(\frac{2\varepsilon\varepsilon_o V_b}{qN}\right)^{1/2} \quad (11)$$

Also, the maximum electric field, E_m is given by [38]

$$E_{\max}=\left(\frac{2qNV_b}{\varepsilon\varepsilon_o}\right)^{1/2} \quad (12)$$

The values of N,V_b, W and E_m at different temperatures are determined and listed in Table 4 for devices 1 and 2. It is observed that the device parameters N, V_b,W and E_m of device 1 is low compared to that for device 2. Moreover, the increase in the carrier concentration of the two deviceswithtemperature can be attributed to the decrease in the width of the depletion region [39].

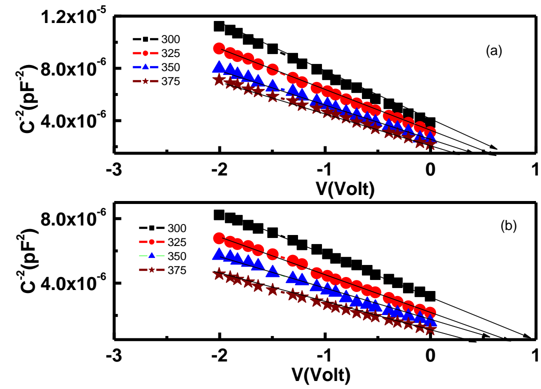

Fig. 14. Capacitance-voltage characteristics of PbTe/n-Si heterojunction in the temperature range 300-375 K a) at substrate temperature 473 K, b) at substrate temperature 503 K.

Table 4. The parameters estimated from C-V and I-V characteristics.

T(K	N_Ax10^{15} (cm^{-3})		V_b(V)		Wx10^{-5} (cm)		$E_{max}10^3$(V/cm)		*n*		Φ_b(eV)	
	D_1	D_2	D_1	D_2	D_1	D_2	D_1	D_2	D_1	D_2	D_1	D_2
300	2.1±0.10	2.91±0.14	0.63 ±0.03	1 .03±0.05	6.4 ±0.32	6.8±0.32	19.6±0.98	30.2±1.51	5.2±0.26	9.3±0.46	0.59 ±0.03	0.51±0.02
325	2.3 ±0.11	3.15±0.15	0.51 ±0.02	0.69±0.03	2.83±0.14	5.3±0.26	18.7 ±0.93	25.8±1.29	5.1±0.25	8.7±0.43	0.62±0.03	0.55±0.03
350	2.7±0.13	3.46±0.17	0.32 ±0.01	0.42±0.02	1.54 ±0.07	3.9±0.19	16.3±0.81	21.1±1.05	4.3 ±0.15	6.7±0.33	0.65 ±0.03	0.58±0.03
375	3.1 ±0.15	4.35±0.21	0.23 ±0.01	0.24±0.01	1 .1 ±0.05	2.7±0.13	14.5 ±0.72	17.8±0.89	3.2±0.16	4.8±0.24	0.67±0.03	0.62±0.03

(D_1 denote device 1 and D_2 denote device 2)

3.7. Current-voltage characterization

The current–voltage (*I–V)* characteristics of the n-PbTe/p-Si heterojunction devices measured in the temperature range from 300 to 375 K are shown in Fig. 15. The forward bias is corresponding to a positive voltage at the p-Si. Some important junction parameters can be extracted using *I-V* characteristics such as rectification ration (*RR*), ideality factor (η) and barrier height (Φ_b). It is clear from this figure that, the two devices have good rectifying property. The rectification ratio, RR, can be calculated from the ratio of forward biasing current/reverse biasing current at a certain applied voltage. As observed from Fig. 16 that the RR obtained for device 2 is found to be higher as compared to the device 1 which may be attributed to the high value of width of the depletion region and barrier height. The value of RR increases with temperature because of the T^2 dependence of I_0. The rectification ratio also changed with voltage; this can be related to the Schottky lowering of the barrier heights due to image force effect [40].

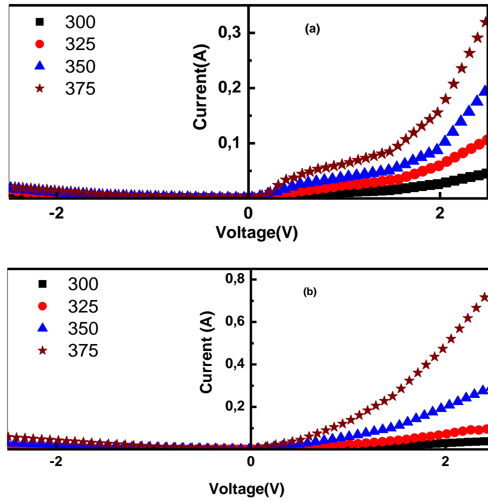

Fig. 15. Current-voltage characteristics of PbTe/n-Si heterojunction in the temperature range 300-375 K a) at substrate temperature 473 K, b) at substrate temperature 503 K.

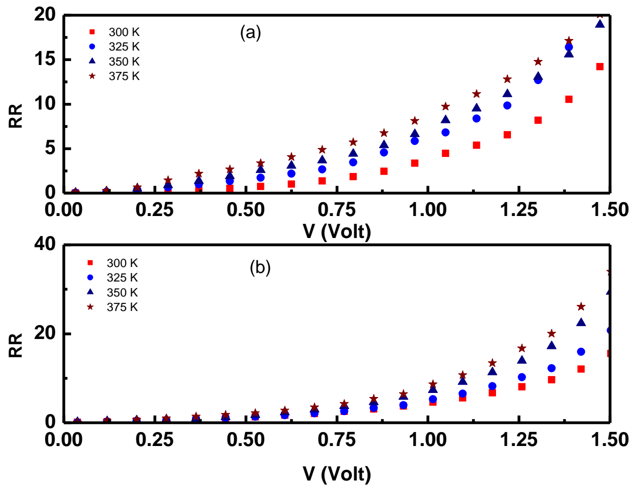

Fig. 16. Plot of rectification ratio (RR) vs. voltage ofPbTe/n-Si heterojunction in the temperature range 300-375 K a) at substrate temperature 473 K , b) at substrate temperature 503 K.

The ideality factor, η, was introduced to take into account the deviation of the experimental *I-V* data from the ideal thermionic model. This factor is calculated from the slope of the linear region of the forward bias of the semilog *I –V* characteristics.

The barrier height (Φ_b) is determined from the extrapolation of the curve to V= 0 and is given by the following relation [39]:

$$\Phi_b = \frac{k_B T}{q}\left(\frac{\ln AA^* T^2}{I_0}\right), \qquad (13)$$

where A^* is the effective Richardson constant, I_0 is the reverse saturation current, q is the electronic charge and k_B the Boltzmann constant.

The values of $\eta$and Φ_b derived at each temperature in the range 300-375 K are listed in Table 4 and shown in Fig. 17. As observed, while Φ_b increases with an increase in temperature, the value of η decreases. Such behavior for the ideality factor and thebarrier height have been attributed to the particular distribution of the interface states or an alternative approach to the lateral inhomogeneities that are found in the Schottky barrier interfaces [40]. A high value of ideality factor is observed at room temperatures. Case ofη greater than unity (η>1) is probably due to a potential drop in the interface layer and the presence of excess current and the recombination current through the interfacial states between the semiconductor/insulator layers [40, 41]. Tatar et al.[42] attributed the behavior for η and Φ_b to the particular distribution of the interface states or an alternative approach to the lateral inhomogeneities that are found in the Schottky barrier interfaces.

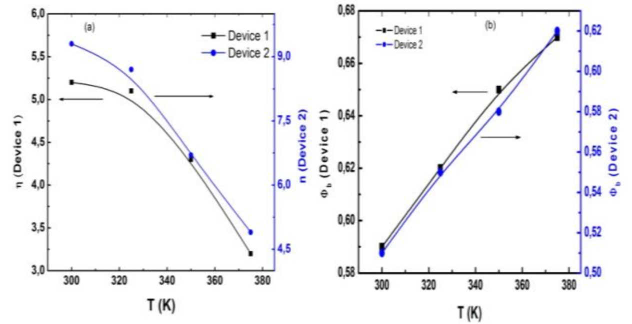

Fig. 17. (a) Plot of ideality factor (n) vs. temperature (T), (b) Plot of barrier height (Φ_b) vs. temperature (T) of PbTe/n-Si heterojunction in the temperature range 300-375 K for the two devices.

To study the predominant conduction mechanism in the n-PbTe/p-Si junctions, different mechanisms are possible such as Schottky emission, Poole-Frenkel, space charge limited (SCLC), etc [38].

The predominant conduction mechanism in n-PbTe/p-Si Schottky diodes could be determined from the power of log*I*–log*V* curve. Power of the curve greater than 2 ($m > 2$) indicates SCLC mechanism whereas being equal to 1 ($m = 1$) implies ohmic character. The power value between 1 and 2 impose Schottky conduction mechanism.

According to the general information above, one can analyze the predominant conduction mechanism in n-PbTe/p-Si junction. As shown in Fig. 16 (a) and (b) for devices 1 and 2, respectively, two linear regions are observed in log*I*–log*V* curve of n-PbTe/p-Sijunction. When the power lies between 1 and 2 impose either Schottky or Poole-Frenkel conduction [38]. For the device 1, Fig. 18 (a), in the lower electric field region ($0.1 < V_F < 0.5$) whereas the power lies in the range 1.3-

1.6, the conduction mechanism might be through either Schottky or Poole-Frenkel conduction mechanism [38]. Concerning the other mechanism is in the higher electric field region ($0.5 < V_F$), where the power is in the range 2-2.35, the current flows by SCLC mechanism. This means that with increasing voltage, more electrons injected from electrode into the film and current density originates from the SCLC mechanism.

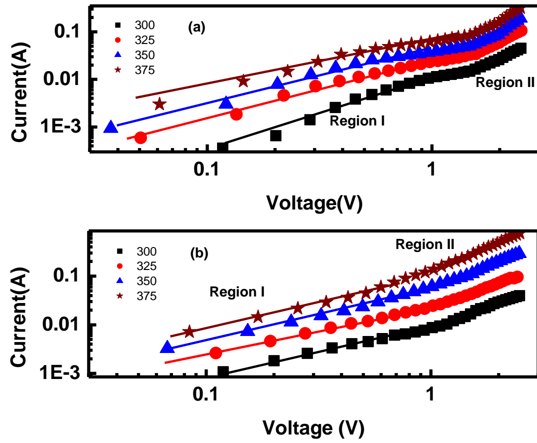

Fig. 18. Current-voltage characteristics of PbTe/n-Si heterojunction in the temperature range 300-375 K a) at substrate temperature 473 K,b) at substrate temperature 503 K.

Using the above information, similar analysis is carried out for determining the predominant conduction mechanism in device 2, Fig. 18 (b). As shown in this figure, two linear regions are presented in *log I–log V* curve. One of them is in the lower electric field region ($0.1<V_F<0.5$) where the power is in the proximity of unity (ohmic mechanism). This may be attributed to the interface barrier blocks the charge injection; hence, the number of charge carrier participating in the current does no increase [43]. The other is in the higher electric field region ($0.5<V_F$), where the power is in the range 1.65-1.85. The conduction mechanism might be through either Schottky or Poole-Frenkel conduction mechanism.

For Schottky and Poole-Frenkel conduction mechanisms, the current equation should be reconsidered as [44]

$$I = AA^{*}T^{2}\exp\left(\frac{\Phi_s}{kT}\right)\exp\left(\frac{\beta\ V^{1/2}}{kTd_s^{1/2}}\right) \quad (14)$$

For the Schottky effect and

$$I = I_0\ \exp\left(\frac{\beta_{PF}V^{1/2}}{kT\ \ d_s^{1/2}}\right) \quad (15)$$

For the Poole-Frenkel effect, where A^* is the Richardson constant, Φ_s is the Schottky depletion height, I_0 is the lower-field current density, and β_s and β_{PF} are the respective Schottky and Poole-Frenkel field-lowering coefficients. Theoretical values of these coefficients are given by

$$2\beta_s = \beta_{PF} = \left(\frac{q^3}{\pi\varepsilon\varepsilon_0}\right)^{1/2} , \quad (16)$$

where ε is the dielectric constant of semiconductor and ε_0 is the permittivity of free space.

For detailed analysis of lower voltage region in device 1 and higher voltage region in device 2 to clarify the conduction mechanism. Fig. 19(a) and (b) shows the plot of ln*I* vs.$V^{1/2}$ for the two devices, which clearly yield a linear section of the curve, could be interpreted in terms of either Schottky emission or Pool-Frenkel emission. Corresponding experimental value of β calculated from the slope of the linear region of Fig. 19(a) was found to be in the range 5× 10^{-5} - 6× 10^{-5} eV$m^{1/2}$ $V^{-1/2}$. The experimental value of β for device 2, derived from the slope of the linear section of Fig.19(b), was found to be in the range 1.6×10^{-5} - 2.2 ×10^{-5} eV$m^{1/2}$ $V^{-1/2}$. Theoretical values of β_s and β_{pf} were found to be 4.8× 10^{-5} eV$m^{1/2}$ $V^{-1/2}$ and 2.4× 10^{-5} eV$m^{1/2}$ $V^{-1/2}$, respectively. Experimental value for β in the device 1 is nearly agreement with the theoretically calculated value of β_{pf}.But experimental value for β in the device 2 is nearly agreement with the theoretically calculated value of β_s. Hence, one can conclude that the conduction mechanism in device1 is controlled by the Poole-Frenkel effect but the Schottky effect is probably conduction mechanism for device 2.

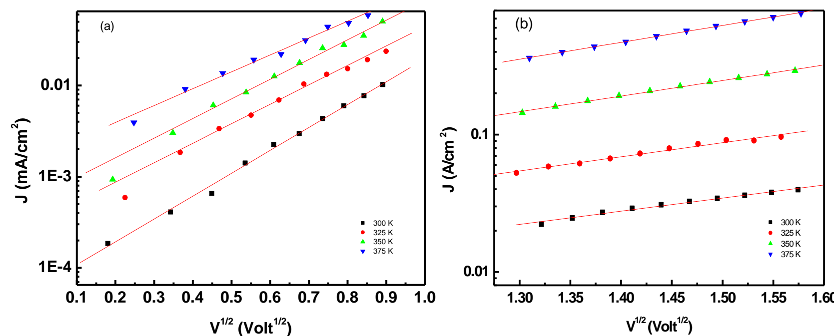

Fig. 19. Plot of current density (J) vs. $V^{1/2}$ of PbTe/n-Si heterojunction in the temperature range 300-375 K a) at substrate temperature 473 K, b) at substrate temperature 503 K.

4. Conclusions

PbTe films deposited at substrate temperature 473 and 503 K have nano-sized structure as checked by SEM, TEM and XRD. The chemical composition of PbTe using EDX showed a nearly stoichiometric composition of sample 2 compared with that for sample 1. The TEM results were in good agreement with the results of the W-H method. The optical characterizations of PbTe thin films were analyzed based on the generation of the envelopes of the interference maxima and minima of the transmission spectrum. The refractive index of PbTe thin films of sample 1 is low compared to that of sample 2 which may be attributed to the surface roughness that affects the optical characteristics due to the presence of light scattering. Moreover, the determined value of the direct band gap of sample 2 was found to be larger than that for sample 1. From the *C-V* characteristics of n-PbTe/p-Si, it was found that the device parameters N, V_b, W and $E_m$of device 1 is lower as compared to device 2. Moreover, the increase in the carrier concentration of the two devices with temperature in the temperature range 300-375 K can be attributed to the decrease in the width of the depletion region. From the *I-V* characteristics of n-PbTe/p-Si, it was found that the RR for device 2 is high compared to that of device 1 which may be attributed to the high value of width of the depletion region and barrier height. While Φ_b increases with an increase in temperature, the value of n decreases. These changes are indicative of deviations from the pure thermionic emission mechanism and there is a current flow, in excess, with respect to the standard thermionic emission theory. Moreover, the conduction mechanism in device 2 is controlled by the Poole-Frenkel effect but the Schottky effect is probably the conduction mechanism for device 1.

References

[1] D. M. Rowe, CRC Handbook of Thermoelectrics, CRC Press, Boca Raton, Florida, USA, 1995.
[2] D. Khokhlov, Lead Chalcogenides Physics and Applications, Taylor and Francis Books, Inc.: London, 2003.
[3] B. Poudel, W. Z. Wang, D. Z. Wang, J. Y. Huang, Z. F. Re, J. Nanosci. Nanotechnol.**6**, 1050 (2006).
[4] Z. H. Dughaish, Physica B **322**,205 (2002).
[5] B. Li, S. Zhang, F. Zhang, L. Zeng, Appl. Phys. A **76**, 965 (2003).
[6] R. N. Tauber, A. A. Machonis, I. B. Cadoff, J. Appl. Phys. **37**, 4855 (1966).
[7] G. Bauer, G. Springholz, in: Duncan G. Steel, L. P. Bayvel (Eds.), Encyclopedia of Modern Optics, Elsevier, Amsterdam, 2005.
[8] Nugraha, K. Suto, O. Itoh, J. Nishizawa, Y. Yokota, J. Crys. Growth **165**, 402 (1996).
[9] P. J. McCann, I. Chao, H. Sachar, D. McAlister, C. Li, X. Fang, H.Wu, K. Namjou, Spectrochim. Acta, Part A **55**, 1999 (1999).
[10] K. G. Kristovskii, A. E. Kozhanov, D. E. Dolzhenko, I. I. Ivanchik, D. Watson, D. R. Khokhlov, Phys. Solid State **46**, 123 (2004).
[11] Z. Nabi, B. Abbar, S. Mecabih, A. Khalfi, N. Amrane, Comp. Mater. Sci. **18**,127 (2000).
[12] Y. Gelbstein, Z. Dashevsky, M. P. Dariel, Physica B **363**,196 (2005).
[13] P. W. Zhu, L. X. Chen, X. Jia, H. A. Ma, G. Z. Ren, W. L. Guo, W. Zhang, G. T. Zou, J. Phys.: Condens. Matter **14**, 11185 (2002).
[14] H. Zogg, K. Alchalabi, D. Zimin, Defence Sci. J. **51**, 53 (2001).
[15] A. Jdanov, J. Pelleg, Z. Dashevsky, R. Shneck, Mater. Sci. Eng. B-Solid State Mater. Adv. Technol. **106**,89 (2004).
[16] A. I. Fedorenko, A. G. Fedorov, A. Y. Sipatov, O. A. Mironov, Thin Solid Films **267**,134 (1995).
[17] A.B . Mandale, Thin Solid Films, **195**, 15 (1991).
[18] M. M. El-Ocker, F. Sharaf, H. M. Talaat, F. Metawe, M. A. El-Sherbiny Solid State Commun.**76**, 1293 (1990).
[19] A. Jacquot, B. Lenoir, M.O. Boffoue, A. Dauscher, Appl. Phys. A**69**, S613 (1999).
[20] F. Xiao, B. Yoo, M. A. Ryanb, K. Lee, N. V. Myung, Electrochim. Acta, Part A **52**, 1101 (2006).
[21] J. R. Slack, J. C. Burfoot, Thin Solid Films **6**, 233 (1970).
[22] M. M. El-Nahass, A. M. A. El-Barry, A. A. Farag, S. Y. El-Soly, Eur. Phys. J. Appl. Phys. **35**, 75 (2006).
[23] A. A. M. Farag, F. S. Terra, G. M. Mahmoud, A. M. Mansour, J. Alloys Compd. **481**,427 (2009).
[24] B. D. Hall, D. Zanchet, D. Ugarte, J. Appl. Cryst. **33**, 1335 (2000).
[25] K. Venkateswarlu, A. Chandra Bose, N. Rameshbabu, Physica B **405**, 4256 (2010).
[26] R. Swanepoel, J. Phys. E, Sci. Instrum. **17**, 896 (1984).
[27] J. C. Manifacier, J. Gasiot, J. P. Fillard, J. Phys. E: Sci. Instrum. **9**, 1002 (1976).
[28] D. K. Fork, F. Armani-Leplingard, J. J. Kingston, G. B. Anderson. Mater. Res. Soc. Symp. Proc. **392**,189 (1995).
[29] K. A. Aly, A. Dahshan, A. M. Abousehly, Philos. Mag. **88**, 47 (2008).
[30] B. Li, S. Zhang, F. Zhang, L. Zhang, Appl.Phys. A **76**, 965 (2003).
[31] T. Wiktorczyk, Thin Solid Films **405**, 238 (2002).
[32] M. M. El-Nahass, A. A. M. Farag, F. Abd-El-Salam, Appl. Surf. Sci. **255**, 9439 (2009).
[33] N. F. Mott, E. A. Davis, Electronic Processes in Non-Crystalline Materials, Clarendon, Oxford, 1971.
[34] X. Li, I. S. Nandhakumar, G. S. Attard, M. L. Markham, D. C. Smith, J. J. Baumberg, Microporous and Mesoporous Mater. **118**, 403 (2009).
[35] M. Baleva, E. Mateeva, M. Momtchilova, J. Phys: condens. Matter **4**, 8997 (1992).
[36] Z .K. Zlatanov, V. D. Vulchev, M. I. Gulmezov, J. Mat. Electron **9**, 301 (1998).
[37] M. Krunks, A. Mere, A. Katerski, V. Milki, J.

Krustok, Thin Solid Films **511-512**, 434 (2006).
[38] S. M. Sze, K. Ng Kwok, Physics of semiconductor devices. Hoboken, New Jersey: John Wiley & Sons, Inc.; 2007.
[39] A. A. M. Farag, I. S. Yahia, T. Wojtowicz, G. Karczewski, J. Phys. D: Appl. Phys. **43**,215102 (2010).
[40] T. Serin, N. Serin, Commun. Fac. Sci. Univ. Series A_2, A_3, **36**, 1 (1987).
[41] A. A. M. Farag, B. Gunduz, F. Yakuphanoglu, W. A. Farooq, Synthetic Metals **160**, 2559 (2010).
[42] B. Tatar, A. E. Bulgurcuoglu, P. Gokdemir, P. Aydogan, D. Yılmazer, O. Ozdemir, K. Kutlu, International journal of hydrogen energy **34**,5208 (2009).
[43] A. A. M. Farag, W. A. Farooq, F. Yakuphanoglu, Microelectronic Engineering **88**, 2894 (2011).
[44] F. E. Cimilli, M. Saglam, A. Turut, Semicond. Sci. Technol. **22**, 851 (2007).

*Corresponding author: alaafaragg@yahoo.com